

# DS-Net: Dynamic Spatiotemporal Network for Video Salient Object Detection

Yuting Su, Member, IEEE, Weikang Wang, Jing Liu, Member, IEEE, Peiguang Jing, Member, IEEE, and Xiaokang Yang, Fellow, IEEE

**Abstract**—As moving objects always draw more attention of human eyes, the temporal motive information is always exploited complementarily with spatial information to detect salient objects in videos. Although efficient tools such as optical flow have been proposed to extract temporal motive information, it often encounters difficulties when used for saliency detection due to the movement of camera or the partial movement of salient objects. In this paper, we investigate the complimentary roles of spatial and temporal information and propose a novel *dynamic spatiotemporal network* (DS-Net) for more effective fusion of spatiotemporal information. We construct a symmetric two-bypass network to explicitly extract spatial and temporal features. A *dynamic weight generator* (DWG) is designed to automatically learn the reliability of corresponding saliency branch. And a *top-down cross attentive aggregation* (CAA) procedure is designed so as to facilitate dynamic complementary aggregation of spatiotemporal features. Finally, the features are modified by spatial attention with the guidance of coarse saliency map and then go through decoder part for final saliency map. Experimental results on five benchmarks VOS, DAVIS, FBMS, SegTrack-v2, and ViSal demonstrate that the proposed method achieves superior performance than state-of-the-art algorithms. The source code is available at <https://github.com/TJUMMG/DS-Net>.

**Index Terms**—Video salient object detection, convolutional neural network, spatiotemporal feature fusion, dynamic aggregation

## I. INTRODUCTION

**V**IDEO Salient Object Detection (VSOD) aims at discovering the most visually distinctive objects in a video. The task of video salient object detection is not only to locate the salient region, but also to focus on the segmentation of salient object, that is, to separate the salient object pixels from the background pixels. Therefore, the results of video salient object detection can be applied to a variety of subsequent computer vision tasks, such as person re-identification [1], visual tracking [2] and video compression [3].

Compared with image salient object detection, video salient object detection is much more challenging because it needs to consider the time continuity between video frames, camera shake, object movement and other factors. In recent years, with the development of convolution neural network (CNN), a variety of learning based salient object detection networks

This work is supported in part by National Science Foundation of China under Grant 61701341 and 61802277.

Y. Su, W. Wang, J. Liu, and P. Jing are with the School of Electrical and Information Engineering, Tianjin University, 300072, China. (E-mails: ytsu@tju.edu.cn, ww\_19970307@tju.edu.cn, jliu\_tju@tju.edu.cn, pgjing@tju.edu.cn.) X. Yang is with MoE Key Lab of Artificial Intelligence, AI Institute, Shanghai Jiao Tong University, Shanghai 200240, China (E-mail: xkyang@sjtu.edu.cn). Corresponding author: Jing Liu.

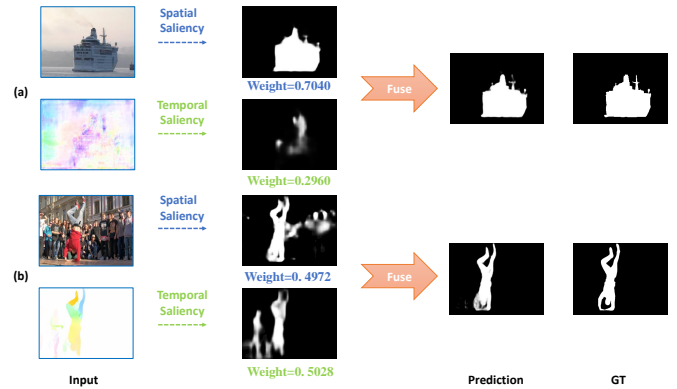


Fig. 1. Illustration of the proposed algorithm for two common yet challenging cases. (a) Noisy optical flow with high spatial contrast. (b) Reliable optical flow with complex spatial background. The DS-Net is capable of efficiently aggregating reliable spatial and temporal information.

have been proposed [4]–[7], which have greatly improved the performance of the algorithms in this field. In video salient object detection task, the motive information between video frames plays a significant role, since the researches have shown that human eyes pay more attention to moving objects in a video [8]. So it is essential to extract motive information in video sequences. At present, a large number of algorithms extract the optical flow [5], [9], which reflects the motion of pixels between two video frames. And the motive information contained in optical flow is often used to guide static saliency for better saliency map. However, in cases where the camera moves, the movement of the salient object is too small, or only part of the salient object is moving, the motive information contained in the optical flow is less correlated with salient objects. Therefore, indiscriminately aggregating the less reliable motive information with spatial information can hardly improve but may even ruin the saliency results.

To address the dynamic reliability of static and motive saliency cues, dynamic aggregation of spatial and temporal information according to their reliability is desired. In this paper, we propose a dynamic spatiotemporal network (DS-Net). The proposed network is composed of four components: symmetric spatial and temporal saliency network, dynamic weight generation, top-down cross attentive aggregation, and final saliency prediction. Symmetric spatial and temporal saliency network explicitly extract saliency-relevant features in static frame and optical flow, respectively. Given the multi-scale spatial and temporal features, a novel dynamic weight generator (DWG) is designed to learn the dynamic weight

vectors representing the reliability of corresponding features, which are then used for top-down cross attentive aggregation (CAA) for each feature. The spatial and temporal saliency maps are also adaptively fused to obtain a coarse saliency map based on the dynamic weight vector. Finally, the coarse saliency map is applied to the progressively dynamically aggregated features via spatial attention to further eliminate background noises and then output the final saliency map.

As shown in Fig. 1, the temporal information captured by optical flow may varies in its reliability for salient object detection. When it fails to reflect the motion of foreground objects, as shown in (a), the proposed DS-Net can adjust the aggregation process so that the spatial branch plays a dominant role. On the contrary, when video frame contains complex background noises while the temporal information is more highly correlated with the foreground object, as shown in (b), the proposed DS-Net performs equally well by emphasizing on the temporal branch via cross attentive aggregation. Experimental results on five large-scale video salient object detection datasets validate the effective of the proposed algorithm. In short, the contributions of this paper are summarized as follows:

- 1) To tackle the dilemma of dynamic reliability of static and motive saliency cues, we propose a dynamic spatiotemporal network (DS-Net) which automatically learns the reliability of spatial and temporal branch and complementarily aggregates the corresponding features in a cross attentive way.
- 2) A dynamic weight generator is designed to fuse multi-scale features and explicitly learn the weight vector representing the reliability of input features, which can be used for aggregating multi-scale spatiotemporal features as well as coarse saliency maps.
- 3) A top-down cross attentive aggregation procedure with non-linear cross thresholding is designed to progressively fuse the complementary spatial and temporal features according to their reliability.

The rest of this paper is organized as follows. Section II reviews existing video salient object detection algorithms and spatiotemporal fusion methods. Section III describes the proposed algorithm thoroughly. Experiment setting as well as evaluation results are discussed in Section IV. Finally, conclusive remarks are made in Section V.

## II. RELATED WORK

### A. Video Salient Object Detection

Image salient object detection has been explored for decades and achieved excellent performance [10]–[12]. Compared with image salient object detection, video salient object detection task is more challenging due to the motion of objects.

Traditional video salient object detection methods usually employed handcrafted features to locate the salient regions [13]–[15]. In recent years, the rapidly developing convolution neural network greatly improves the performance of video salient object detection algorithms. Wang et al. [7] firstly applied the fully convolution neural (FCN) network to video salient object detection and achieved remarkable performance.

After that, more and more deep learning based methods have been proposed. Li et al. [5] extended the FCN-based image saliency model by the flow guided feature warp and recurrent feature refinement module. Afterwards, to get better spatiotemporal feature fusion performance, Song et al. [4] directly input sequences into two parallel dilated bi-directional ConvLSTMs to learn spatiotemporal information and obtained significant performance improvement. Following previous works, Fan et al. [6] used parallel dilated convolution layers to exploit multi-scale information and equips convLSTM with a saliency-shift-aware attention mechanism. Some works also investigate the guidance role of motive features to static features. Li et al. [9] proposed a novel motion guided network taking single static frame and optical flow as input, which can achieve excellent performance. Recently, some works started to focus on designing lightweight VSOD networks. Gu et al. [16] proposed a novel self-attention mechanism based on non-local block and utilized pyramid structure to get motion cues in different scales and different speed, which achieved state-of-art performance as well as the highest fps among all other learning based VSOD algorithms.

### B. Fusion of Spatiotemporal Information

The optimization of fusion and extraction strategy of spatiotemporal information is always of the first importance in video saliency detection. In the early days, conventional algorithms mainly relied on techniques including low-rank and sparse decomposition [17], local gradient flow [18], object proposals [19] and so on. At present, there are generally three main categories of spatiotemporal fusion strategies in learning based video saliency detection methods: direct temporal fusion, recurrent fusion, and bypass fusion.

Representative models for direct temporal fusion are [7], [20], which used FCN to extract spatial features of different frames and directly concatenate them together to fuse spatiotemporal information. This simple connection fails to effectively reflect the correlation between spatial and temporal features. For recurrent fusion, the convolutional memory units such as ConvLSTM and ConvGRU are usually used to integrate sequence information in a recurrent manner. Representative models include [6], [21] and [22] which employed ConvLSTM and ConvGRU respectively to aggregate long-range spatiotemporal features. Compared with direct temporal fusion, these memory units can extract the temporal continuity by inputting consecutive frames in order. However, these memory units often lead to high computational and memory cost. The last type of spatiotemporal fusion employs different bypasses to explicitly extract static and motion information and then fuse features from different bypasses together. The most commonly used method to represent temporal motion is to calculate optical flow between consecutive frames. Li et al. [9] proposed a novel motion attention based on optical flow to guide the spatial feature extraction and realize the fusion of spatiotemporal features. This fusion method is simple and effective, but it is highly sensitive to the accuracy of optical flow. Noticing this drawback and being aware of the complex human visual attention mechanism, we propose to

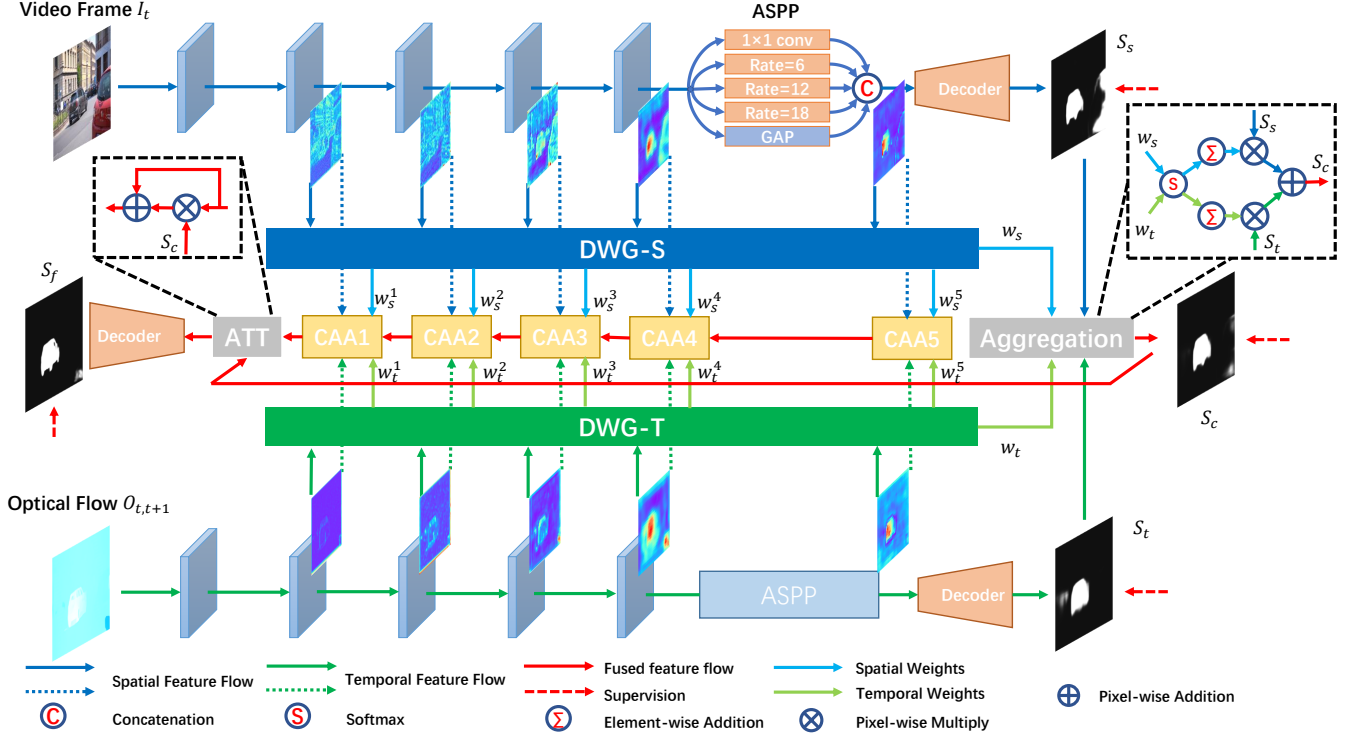


Fig. 2. Overview of the proposed dynamic spatiotemporal network (DS-Net). DWG-S and DWG-T: dynamic weight generator for spatial and temporal branch. CAA: cross attentive aggregation module.

dynamically fuse spatial and temporal information according to input sequences. In this discriminate way, both spatial and temporal features can show their strength without interfering with each other.

### III. THE PROPOSED ALGORITHM

The whole network structure is illustrated in Fig. 2. We propose a dynamic spatiotemporal network which can adaptively aggregate the spatial information from static video frame and the temporal information from optical flow. Firstly, the video frame and the optical flow between the current and next frame are input into the symmetric saliency network to extract spatial and temporal motive features, respectively. After that, a dynamic weight generator is used to fuse features of different scales and generate weight vectors. The weight vectors are used to dynamically aggregate multi-scale spatial and temporal features as the final spatiotemporal features. Finally, through a top-down cross attentive feature fusion procedure, the multi-scale spatiotemporal features are progressively fused for the final saliency maps. In addition, the spatial and temporal saliency maps are also fused adaptively for a coarse saliency map based on the weight vector. And the coarse saliency map is used to suppress the background noises of spatiotemporal feature via spatial attention.

#### A. Symmetric Spatial and Temporal Saliency Network

As shown in Fig. 2, the DS-Net mainly includes two symmetric branches, which are used to explicitly extract static spatial features and motive temporal features respectively.

Motivated by [23], these two branches are both composed of a ResNet34 [24] feature extractor, an Atrous Spatial Pyramid Pooling (ASPP) [25] module and a decoder. We adopt the head convolution and four residual structures of classic ResNet34 as feature extractor. After that, the feature is input into the ASPP module for multi-scale information extraction. As shown in Fig. 2, ASPP module mainly uses four convolution kernels of different receptive fields to extract multi-scale information. The convolution kernels of different receptive fields are realized by different dilation rates. Then, the four features representing multi-scale information are concatenated with the feature after global average pooling to obtain the final output feature. Finally, the feature after ASPP module is input into the decoder to generate saliency prediction map. The decoder used in this paper contains three convolution and activation layers to realize channel reduction.

For the ease of the following descriptions, denote the current frame as  $I_t$  and the next frame as  $I_{t+1}$ . These two images are input into FlowNet2.0 [26] to generate the optical flow image, which is denoted as  $O_{t,t+1}$ . Then  $I_t$  and  $O_{t,t+1}$  go through the symmetric spatial and temporal saliency network to extract features and predict coarse saliency maps. The spatial features output by four residual structures of ResNet34 and ASPP module are denoted as  $\mathcal{F}_s = \{f_s^i | i = 1, \dots, 5\}$ . Similarly, the output features of the temporal branch are denoted as  $\mathcal{F}_t = \{f_t^i | i = 1, \dots, 5\}$ . The coarse spatial and temporal saliency map are denoted as  $S_s$  and  $S_t$ .

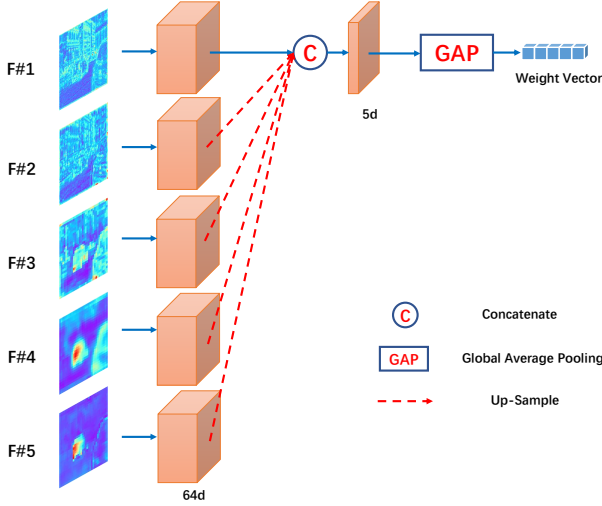


Fig. 3. The structure of dynamic weight generator. F#*i* denote the features extracted from the *i*-th layer of spatial or temporal saliency branch.

## B. Dynamic Weight Generator

The structure of the proposed dynamic weight generator is illustrated in Fig. 3. Researches have shown that features from different layers of the network contain complementary global context and local detailed information [27], [28]. Therefore, the multi-scale features captured from spatial or temporal branch are jointly employed to generate weight vectors. In this way, the information of different scales of features are effectively fused, so that the learned weight vectors can better reflect the relative reliability of different features.

Given the feature pyramid  $\mathcal{F}_s$  or  $\mathcal{F}_t$  extracted from symmetric saliency network, a convolution layer is first applied to transform all feature maps into channel of 64. Afterward, four deeper but coarser-scale features are upsampled to the finest scale and concatenated with the feature at the finest scale to get a feature with 320 channels. Finally, it goes through a channel reduction layer and global average pooling (GAP) to get a 5-d weight vector. Let  $w_s = [w_s^1, w_s^2, w_s^3, w_s^4, w_s^5]$  and  $w_t = [w_t^1, w_t^2, w_t^3, w_t^4, w_t^5]$  represent the 5-d weight vector for spatial and temporal branch respectively. As will be shown later, the 5-d weight vectors correspond to the reliability of 5 input features, which will be used for the subsequent attentive feature fusion as well as the coarse saliency maps fusion.

## C. Cross Attentive Aggregation

As mentioned above, human attention is driven by both static cues and motive cues, but their contributions to salient object detection vary from sequences to sequences. Therefore, it is desired to dynamically aggregate the spatial and temporal information. Recall that the dynamic weights  $w_s^i$  and  $w_t^i$  are learned to stand for the relative reliability of their corresponding features  $f_s^i$  and  $f_t^i$ . A straightforward way to get spatiotemporal feature is the weighted summation as:

$$F_{agg}^i = w_s^i \cdot f_s^i + w_t^i \cdot f_t^i. \quad (1)$$

Although it seems reasonable, there is a key risk of unstable weighting. As  $w_s$  and  $w_t$  are derived separately from two

independent networks with totally different inputs (i.e., static frame and optical flow), there is no guarantee that  $w_s$  and  $w_t$  can serve as the weighting factor, in other word, being comparable. Therefore, the naive aggregation approach of (1) may result in unstable weighting of spatial and temporal information.

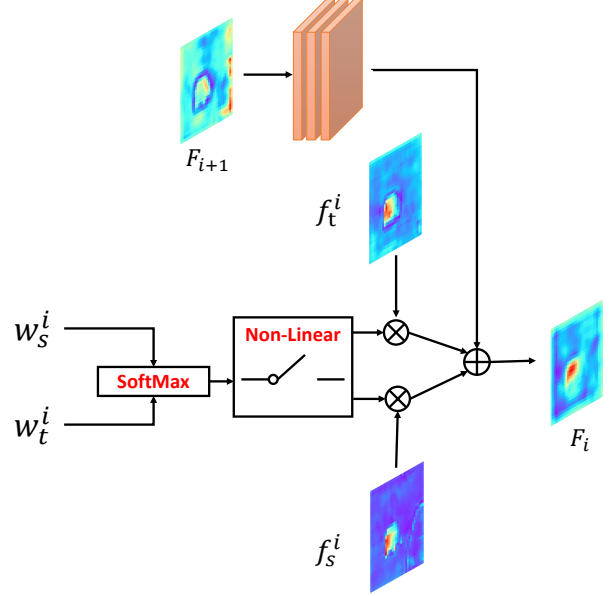


Fig. 4. Illustration of cross attentive aggregation.

To address this issue, instead of direct aggregation using independent weight vectors, we propose a simple yet efficient cross attentive aggregation scheme to jointly evaluate the relative reliability of spatial and temporal features. Fig. 4 illustrates the top-down cross attentive feature aggregation of coarser scale feature  $F_{i+1}$  with spatial feature  $f_s^i$  and temporal feature  $f_t^i$ . As shown in the figure, the spatial and temporal dynamic weights  $w_s^i$  and  $w_t^i$  are first normalized with ‘cross’ softmax, making them ranging from 0 to 1 with the summation of 1. Denote the regularized dynamic weight vector as  $v_s$  and  $v_t$  for spatial and temporal branch respectively, we have:

$$\begin{aligned} v_s^i &= \frac{e^{w_s^i}}{e^{w_s^i} + e^{w_t^i}} \\ v_t^i &= \frac{e^{w_t^i}}{e^{w_s^i} + e^{w_t^i}}. \end{aligned} \quad (2)$$

Another benefit of applying softmax is to exaggerate the gap between spatial and temporal reliability. As mentioned above, it is highly likely that one single saliency cue (spatial or temporal) is obviously much better than the other. In this case, indiscriminate aggregation of the poor saliency branch will heavily degrade the overall performance even if the other saliency cue performs excellently. To further suppress the distracting impact from the noisy or invalid saliency branch, a non-linear cross thresholding is proposed as:

$$(u_s^i, u_t^i) = \begin{cases} (0, v_t^i) & v_t^i - v_s^i > \tau \\ (v_s^i, 0) & v_t^i - v_s^i < -\tau \\ (v_s^i, v_t^i) & otherwise \end{cases}, \quad (3)$$

where  $\tau$  is a threshold. The generated dynamic weights  $u_s^i$  and  $u_t^i$  are then used to weight the corresponding features extracted from spatial and temporal branches for complementary spatiotemporal features, which can be expressed as:

$$F_{agg}^i = u_s^i \cdot f_s^i + u_t^i \cdot f_t^i. \quad (4)$$

It is worth noting that compared with existing cross attention modules [29], [30] where complex operations such as correlations are generally carried out on the whole feature maps, the proposed cross attentive aggregation is of extremely low complexity since the interaction between two-bypass network are carried out on the 5-d dynamic weight vector, which can also be easily obtained as described above. As will be demonstrated by the experiments, the simple yet efficient cross operations of softmax and non-linear thresholding can well determine the relative reliability of spatial and temporal saliency branch, enhancing the final performance.

TABLE I

THE PARAMETERS OF THREE CONVOLUTION KERNELS IN FIVE CAA MODULES. ‘KS’, ‘PD’ AND ‘CHN’ DENOTE THE KERNEL SIZE, PADDING AND OUTPUT CHANNEL NUMBERS, RESPECTIVELY.

	Conv1			Conv2			Conv3		
	ks	pd	chn	ks	pd	chn	ks	pd	chn
CAA 1	3	1	64	3	1	64	3	1	64
CAA 2	3	1	128	3	1	128	3	1	64
CAA 3	5	2	256	5	2	256	5	2	128
CAA 4	7	3	512	7	3	512	7	3	256
CAA 5	3	1	256	3	1	256	3	1	512

For the coarse scale feature  $F_{i+1}$ , it first goes through three convolution layers to gradually reduce the channel number to match that of spatiotemporal feature at current scale  $F_{agg}^i$ . The parameters of convolution kernels in five CAA modules are listed in Table I. Then, the coarse scale feature is upsampled to match the resolution of  $F_{agg}^i$ . The final progressive aggregation can then be formulated as:

$$F_i = \mathcal{T}(F_{i+1}) + F_{agg}^i, \quad i = 1, 2, 3, 4, \quad (5)$$

where  $\mathcal{T}(\cdot)$  stands for three convolution layers and one upsampling layer. For the coarsest scale  $i = 5$ , only current scale of features are available, so  $F_5 = F_{agg}^5$ . The final output feature after the proposed top-down progressive aggregation scheme can be denoted as  $F_{final} = \mathcal{T}(F_1)$ .

#### D. Spatial Attention based on Coarse Saliency Map

In the dynamic weight generation module, the 5-d weight vectors are learned to represent the reliability of input saliency features. When the feature extracted by one branch is better than that from the other branch, larger weights are assigned to it. Otherwise, smaller weights are assigned. Under this circumstance, the 5-d vectors  $u_s^i$  and  $u_t^i$  as a whole can be regarded as the reliability for the corresponding spatial and temporal saliency branch. Therefore, we sum up the 5-d vector to get the dynamic reliability weight for the corresponding saliency map. Given the spatial saliency map  $S_s$  and temporal saliency map  $S_t$ , the coarse saliency map is derived as:

$$S_c = \epsilon_s \cdot S_s + \epsilon_t \cdot S_t, \quad (6)$$

where  $\epsilon_s = \frac{\sum v_s^i}{\sum v_s^i + \sum v_t^i}$ ,  $\epsilon_t = \frac{\sum v_t^i}{\sum v_s^i + \sum v_t^i}$  are the reliability weights for the corresponding branches.

As shown in Fig. 2, motivated by [9], the coarse prediction map is adopted as an accurate guidance to suppress background noises of spatiotemporal feature  $F_{final}$ . The output feature  $F_{att}$  can be written as:

$$F_{att} = F_{final} \cdot S_c + F_{final}. \quad (7)$$

Finally, the feature map  $F_{att}$  is passed to a decoder to get the final saliency map  $S_f$ .

The benefit to generate the coarse saliency map in attentive way is two-fold: 1) Through dynamic weighting the coarse spatial and temporal saliency maps, a more reliable coarse saliency map can be generated, which can facilitate more effective spatial attention. 2) As the dynamic weight for spatial and temporal coarse saliency map is the sum of weight vectors, it will promote the adaptive learning of the weight vectors with multiple supervision in the training process.

#### E. Loss Function

Without loss of generality, as the proposed saliency model is with multiple saliency outputs, the network is trained in a multiple supervision manner for quick convergence and superior performance. The overall loss function is composed of four components from three coarse saliency maps and the final saliency map. Cross entropy losses are adopted, which are defined as:

$$l = -\frac{1}{N} \left[ \sum_{k \in Y_+} \log S(k) + \sum_{k \in Y_-} \log (1 - S(k)) \right], \quad (8)$$

where  $Y$  denotes the saliency ground truth, and  $N$  is the total number of pixels in the input image.  $S$  is the predicted saliency map.  $Y_+$  and  $Y_-$  denote the positive part and negative part of the ground truth respectively. Let the  $l_s$ ,  $l_t$ ,  $l_c$ , and  $l_f$  represent the losses between the saliency groundtruth and the three coarse saliency maps  $S_s$ ,  $S_t$ ,  $S_c$  and final saliency map  $S_f$ , respectively. The total loss function of the network is calculated as:

$$L = l_s + l_t + l_c + l_f. \quad (9)$$

## IV. EXPERIMENTAL RESULTS

### A. Implementation

The proposed model is built based on pytorch repository. We initialize ResNet34 in symmetric spatial and temporal saliency network with the weights of ResNet34 pretrained on ImageNet [31]. And we trained our model on the training set of one image dataset DUTS [32] and three video dataset DAVIS [33], FBMS [34] and VOS [35]. Considering that the input of our network includes optical flow images, for the image dataset, the input optical flow images are filled with zeros, which means that these frames do not contain motion information.

During the training process, we first resize all input images to  $512 \times 512$ . The Adam [36] optimizer with initial learning rate  $5e-5$ , a weight decay of 0.0005 and an momentum of 0.9 is used to train our model. And the training batch size is set to

TABLE II

COMPARISON WITH STATE-OF-THE-ART VIDEO SALIENT OBJECT DETECTION ALGORITHMS. "↑" MEANS LARGER IS BETTER AND "↓" MEANS SMALLER IS BETTER. "-" INDICATES THE MODEL HAS BEEN TRAINED ON THIS DATASET. "-" REPRESENTS THE TRADITIONAL METHODS. "\*" DENOTES THAT THIS ALGORITHM HAS ACCESSED TO UNFIXED BACKBONES. THE TOP TWO METHODS ARE MARKED IN RED AND BLUE, RESPECTIVELY.

Method		MBD	MSTM	STBP	SCOM	SCNN	FCNS	FGRNE	PDB	SSAV	MGA	PCSA	ours
Backbone		-	-	-	-	VGG	VGG	*	ResNet50	ResNet50	ResNet101	MobileNet	ResNet34
DAVIS	maxF ↑	0.470	0.429	0.544	0.783	0.714	0.708	0.783	0.855	0.861	<b>0.892</b>	0.880	<b>0.891</b>
	S ↑	0.597	0.583	0.677	0.832	0.783	0.794	0.838	0.882	0.893	<b>0.912</b>	0.902	<b>0.914</b>
	MAE ↓	0.177	0.165	0.096	0.048	0.064	0.061	0.043	0.028	0.028	<b>0.022</b>	<b>0.022</b>	<b>0.018</b>
FBMS	maxF ↑	0.487	0.500	0.595	0.797	0.762	0.759	0.767	0.821	0.865	<b>0.907</b>	0.831	<b>0.875</b>
	S ↑	0.609	0.613	0.627	0.794	0.794	0.794	0.809	0.851	0.879	<b>0.910</b>	0.866	<b>0.895</b>
	MAE ↓	0.206	0.177	0.152	0.079	0.095	0.091	0.088	0.064	0.040	<b>0.026</b>	0.041	<b>0.034</b>
ViSal	maxF ↑	0.692	0.673	0.622	0.831	0.831	0.852	0.848	0.888	0.939	<b>0.940</b>	<b>0.940</b>	<b>0.950</b>
	S ↑	0.726	0.749	0.629	0.762	0.847	0.881	0.861	0.907	0.939	0.941	<b>0.946</b>	<b>0.949</b>
	MAE ↓	0.129	0.095	0.163	0.122	0.071	0.048	0.045	0.032	0.020	<b>0.016</b>	0.017	<b>0.013</b>
VOS	maxF ↑	0.562	0.336	0.403	0.690	0.609	0.675	0.669	0.742	0.742	0.745	<b>0.747</b>	<b>0.801</b>
	S ↑	0.661	0.551	0.614	0.712	0.704	0.760	0.715	0.818	0.819	0.806	<b>0.827</b>	<b>0.855</b>
	MAE ↓	0.158	0.145	0.105	0.162	0.109	0.099	0.097	0.078	0.073	0.070	<b>0.065</b>	<b>0.060</b>
SegV2	maxF ↑	0.554	0.526	0.640	0.764	-	-	-	0.800	0.801	<b>0.828</b>	0.810	<b>0.832</b>
	S ↑	0.618	0.643	0.735	0.815	-	-	-	0.864	0.851	<b>0.885</b>	0.865	<b>0.875</b>
	MAE ↓	0.146	0.114	0.061	0.030	-	-	-	<b>0.024</b>	<b>0.023</b>	0.026	0.025	0.028

8. The proposed model is easy to train where all parameters are trained by a simple one-step end-to-end strategy except for the backbone ResNet34 feature extractor. Experiments are performed on a workstation with an NVIDIA GTX 1080Ti GPU and a 2.1 GHz Intel CPU.

## B. Datasets and Evaluation Criteria

1) Dataset: We evaluate our model on five public video salient object detection benchmark datasets, including DAVIS, FBMS, ViSal [18], SegTrackV2 [37], and VOS. DAVIS is a frequently used dataset, which contains 50 videos with totally 3,455 high-quality pixel-wise annotation frames. FBMS is a dataset containing 59 videos with 720 sparsely annotated frames. ViSal is a dataset only used for test containing 19 videos with 193 pixel-wise annotation frames. VOS is a large-scale dataset with totally 200 videos and 7,467 pixel-wise annotated frames. SegTrackV2 is an early adopted dataset with 14 videos and 1,065 annotated frames. In this paper, the test is carried out on the testing part of DAVIS, FBMS, VOS and the whole datasets of ViSal and SegTrackV2.

2) Evaluation Criteria: Mean absolute error (MAE), structure-measure (S-m) [38], max F-measure (maxF) [39] and precision-recall (PR) curves are adopted as the evaluation metrics. MAE is defined as the average pixel-wise difference between the binary ground truth and the saliency prediction map. F-measure is defined as

$$F_{\beta} = \frac{(1 + \beta^2) \cdot Precision \cdot Recall}{\beta^2 \cdot Precision + Recall}, \quad (10)$$

where the  $\beta^2$  is always set to 0.3 in salient object detection task. We report the maximum F-measure (maxF) computed from the PR curve. The S-measure is a newly proposed measurement focusing on the structural similarity between

saliency groundtruth and prediction map. For the PR curves, we firstly threshold the output saliency map into a binary map and match it with the groundtruth. And then, by applying different thresholds to the saliency map, a series of precision and recall pairs are obtained to draw the PR curve.

## C. Performance Comparison

Our proposed method is compared with 11 state-of-the-art methods, including 4 conventional methods: MBD [40], MSTM [41], STBP [42], SCOM [43] and 7 learning based methods: SCNN [44], FCNS [7], FGRNE [5], PDB [4], SSAV [6], MGA [9], PCSA [16]. We use the evaluation code provided by [6] for fair comparison. The maxF, S-measure, and MAE results are listed in Table II and the PR Curves are shown in Fig 6. As shown by Table II, our method achieves the best performance on DAVIS, ViSal, and VOS and the second best performance on FBMS and SegV2. For DAVIS, the proposed method outperforms the second best model MGA by 0.4% in S-measure and 18.2% in MAE. For ViSal, our algorithm surpasses the second best model PCSA by 1.1% in maxF and 0.3% in S-measure. As for VOS, the proposed method significantly outperforms the second best method PCSA by 7.2% in maxF and 3.4% in S-measure. And it achieves a significant performance gap than state-of-the-art algorithms in terms of PR curve. Our method also obtains the highest maxF and second highest S-measure on SegV2. Since we don't train our model on ViSal and SegV2, the competitive and even superior performance on these two datasets validates the generalization capability of the proposed algorithm.

Fig. 5 gives visual comparison of saliency maps with state-of-the-art algorithms. Five diverse yet challenging cases are included. From the top to bottom are cases with complex background (i.e., the crowd and partial occlusion in the 1st and

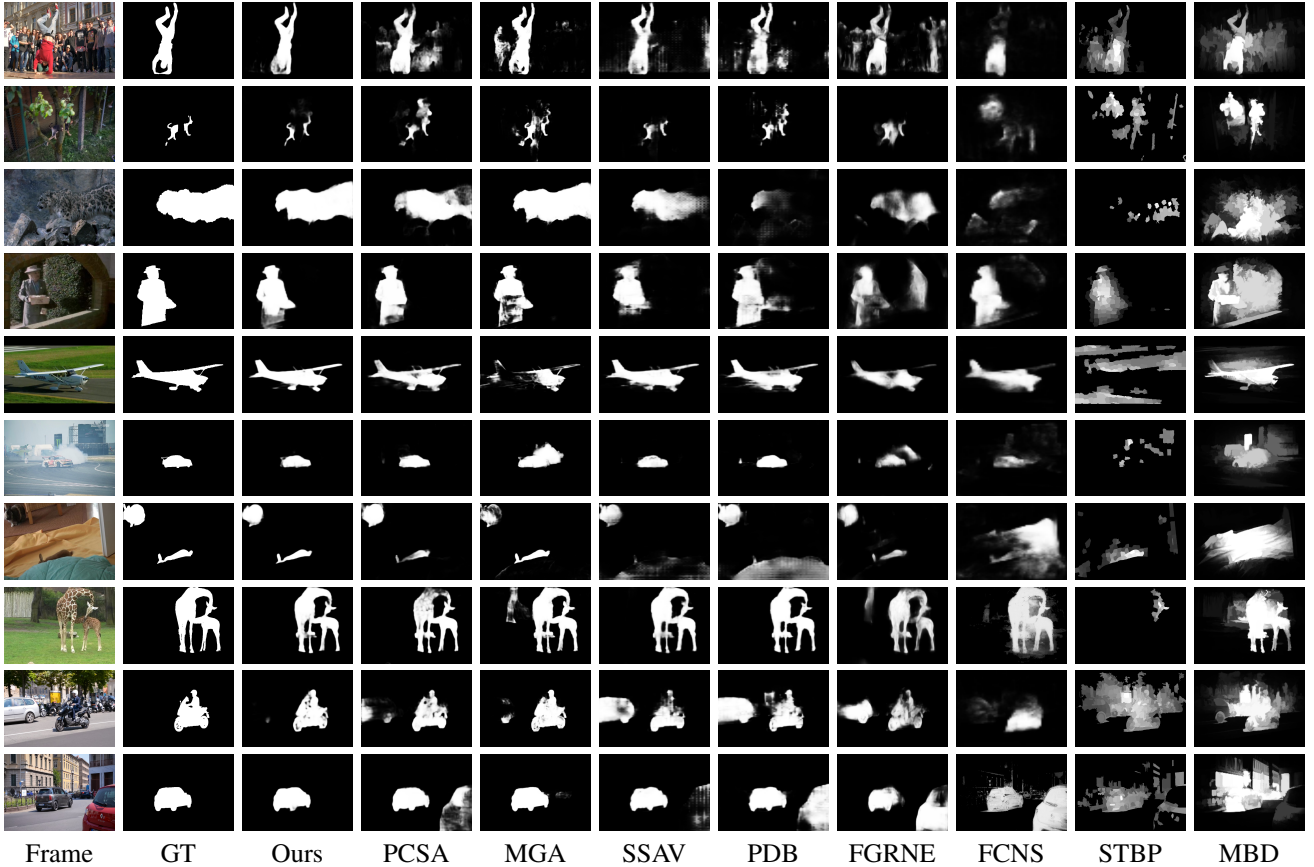


Fig. 5. Visual comparison with state-of-the-art video salient object detection methods.

2nd rows), poor static saliency cue (i.e., low color contrast in the 3rd and 4th rows), poor dynamic saliency cue (i.e., moving camera in 5th and 6th rows), multiple salient objects (i.e., two rabbits and two giraffes in 7th and 8th rows), and distracting non-salient object (i.e., vehicles on road in 9th and 10th rows). It is obvious that our method can accurately segment salient objects in all these cases, demonstrating its efficiency and generalization capability.

As shown in Table II, Fig. 5 and Fig. 6, MGA is the most competitive state-of-the-art algorithm, which also utilized optical flow to extract motion information and a two-branch structure to get complementary spatiotemporal features. However, MGA adopts a more complex backbone network of ResNet101 while the proposed algorithm adopts ResNet34 to extract spatial information. As deeper and more complicated structure always obtain better feature extraction at the cost of higher computational complexity and generally higher difficulty to converge, the competitive and even higher SOD performance of the proposed algorithm validates the effectiveness of the proposed dynamic fusion of spatiotemporal information.

#### D. Sensitivity of Hyper-parameter

Note that the proposed algorithm automatically generates the dynamic weights based on spatial and temporal features, so the only key hyper-parameter of our algorithm is the non-linear threshold  $\tau$  in CAA. The non-linear cross thresholding is designed to suppress the inference from poor saliency cues

TABLE III  
ABLATION STUDY OF THE PROPOSED DS-NET. THE PERFORMANCE ARE TESTED ON LARGE-SCALE DATASET DAVIS.

	M1	M2	M3	M4	M5 (DS-Net)
Baseline	✓	✓	✓	✓	✓
DWG		✓	✓	✓	✓
CAA			✓	✓	✓
Attention				✓	✓
Multi-supervision					✓
maxF $\uparrow$	0.875	0.876	0.877	0.882	<b>0.891</b>
S $\uparrow$	0.906	0.906	0.907	0.910	<b>0.914</b>

where  $\tau$  affects the degree of suppression. Small  $\tau$  may lead to over suppression of informative saliency cue while large  $\tau$  may weaken the suppression ability on distracting information of non-linear cross thresholding. We train the proposed model with different thresholds and the results are shown in Fig. 7. As  $\tau = 0.6$  achieves the best performance, it is set to 0.6 empirically throughout this paper.

#### E. Ablation Study

In this section, we first explore the effectiveness of each key module of the propose algorithm in an incremental manner and then specifically study the effectiveness of each key module's structure in detail. For fair comparison, we propose a baseline model where the spatial and temporal features

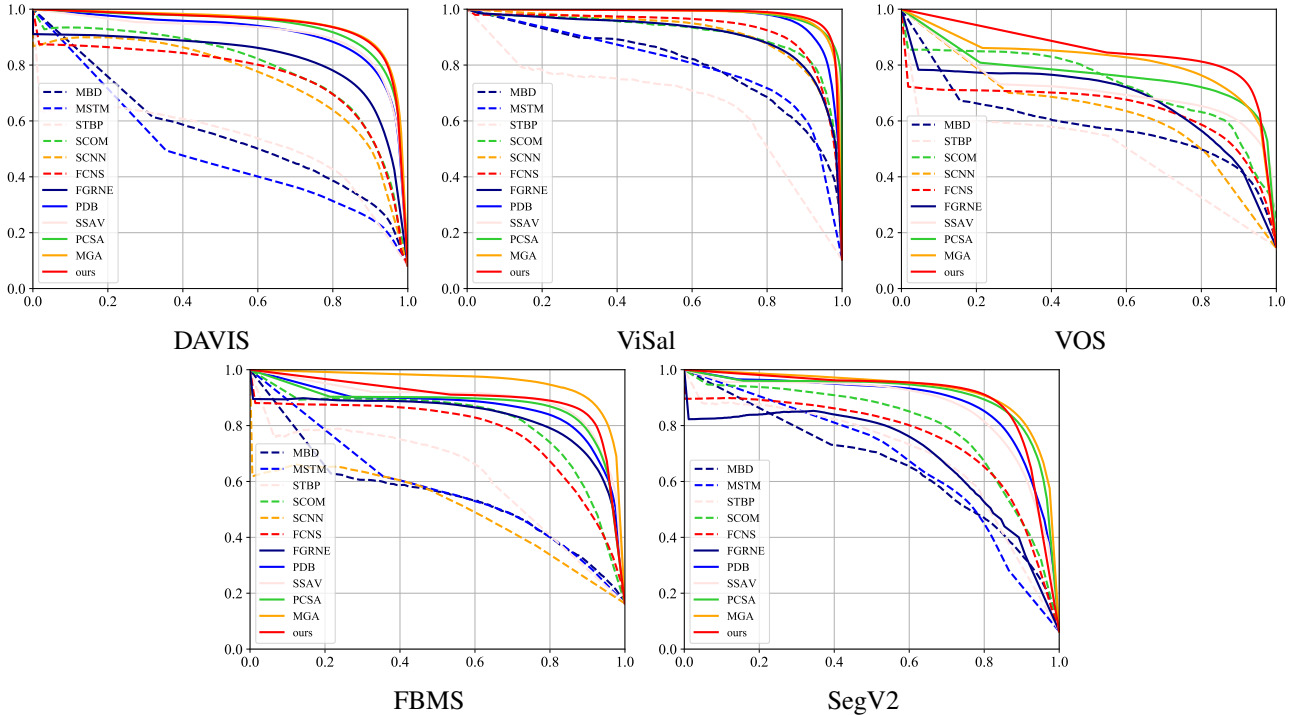


Fig. 6. Precision (vertical axis) recall (horizontal axis) curves on five popular video salient object datasets.

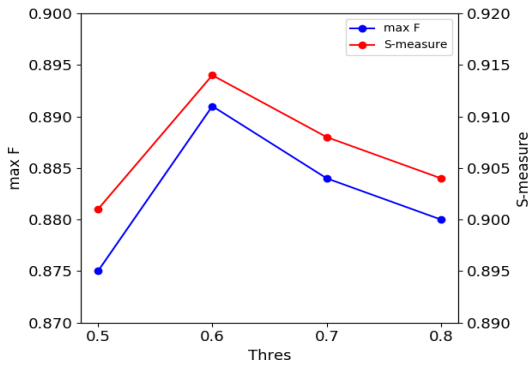


Fig. 7. Sensitive analysis on non-linear threshold  $\tau$ . The performance is tested on DAVIS dataset.

from the same scale of symmetric feature extraction branch are directly summed up and fed into finer scale. Upon this baseline model, the module of DWG, CAA, Spatial Attention, and Multi-supervision are gradually incorporated to obtain the proposed DS-Net. The maxF and S-measure performance on the DAVIS dataset is listed in Table III. It is found that the performance is gradually improved as various modules are successively added to the baseline model. So each key module of the proposed model is effective. In order to further prove the effectiveness of each module, we conduct a series of experiments for each component in our model on three representative datasets, including the commonly used DAVIS dataset, the large-scale VOS dataset and the ViSal dataset which is used only for testing.

TABLE IV  
ABLATION STUDY OF THE PROPOSED DYNAMIC WEIGHT GENERATOR.

		DWG-SEP	DWG-FC	Proposed
DAVIS	maxF $\uparrow$	0.881	0.877	<b>0.891</b>
	S $\uparrow$	0.906	0.907	<b>0.914</b>
	MAE $\downarrow$	0.021	0.020	<b>0.018</b>
ViSal	maxF $\uparrow$	0.932	0.932	<b>0.950</b>
	S $\uparrow$	0.935	0.939	<b>0.949</b>
	MAE $\downarrow$	0.019	0.018	<b>0.013</b>
VOS	maxF $\uparrow$	0.792	0.796	<b>0.801</b>
	S $\uparrow$	0.848	0.852	<b>0.855</b>
	MAE $\downarrow$	0.061	0.064	<b>0.060</b>

1) Dynamic Weight Generator: To demonstrate the effectiveness of the proposed Dynamic Weight Generator, we explore two variants of weight generation strategy. The first variant is denoted as DWG-SEP where the feature of each scale is separately processed by global average pooling and convolution to generate a scalar. The second variant is denoted as DWG-FC where the multi-scale features are concatenated but directly passed through a global average pooling layer and a fully connected layer. The performance of these two variants on three datasets are compared with the proposed model in Table IV. The effectiveness of the proposed DWG for boosting the performance is clearly validated by the consistent improvement on all three datasets. The proposed DWG achieves an average performance gain of 1.40% in maxF and 1.20% in S-measure over DWG-SEP. As for DWG-FC,



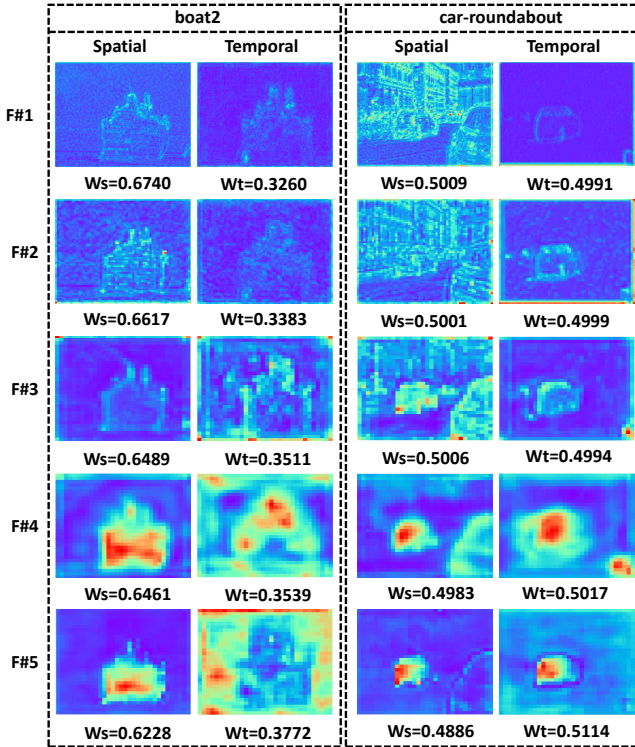


Fig. 8. Feature maps of different depth of layers and their corresponding weights generated by the proposed DWG. F#i represents the feature maps of ith layers. Ws and Wt represent the weights of the feature of spatial and temporal branches respectively.

the proposed structure also brings an average increment of 1.38% in maxF and 0.73% in S-measure. DWG-SEP performs even worse than DWG-FC because it fails to consider the correlation among multi-scale features.

As mentioned above, the weight vector generated by DWG is later used for spatiotemporal feature fusion as it is supposed to indicate whether the corresponding features are in favor of the locating of salient objects. In order to validate this point, we illustrate the feature maps of five different scales in the spatial and temporal branches respectively as well as the corresponding weights generated by the proposed DWG module in Fig. 8. Two different situations are considered: the features extracted from flow map are quite noisy in ‘boat2’ while the temporal features can greatly reflect the movement of foreground object in ‘car-roundabout’. The visualization results show that higher weights are assigned to features more highly correlated to the foreground objects. Therefore, the generated weights can effectively guided the feature fusion process by emphasizing on saliency relevant features. Moreover, it is shown that the weighting process works equally well for features from coarse scale to fine scale, hence, guiding the progressive feature fusion in depth.

2) Cross Attentive Aggregation: To demonstrate the effectiveness of the proposed Cross Attentive Aggregation module, it is compared with three different aggregation methods. The first and second aggregation modules discard the softmax and nonlinear operation of CAA respectively, which is denoted as CAA-woS and CAA-woN. The third aggregation method is

TABLE V  
ABLATION STUDY OF THE PROPOSED CROSS ATTENTIVE AGGREGATION MODULE.

		CAA-woS	CAA-woN	CAA-BU	Proposed
DAVIS	maxF $\uparrow$	0.883	0.877	0.866	<b>0.891</b>
	S $\uparrow$	0.909	0.905	0.898	<b>0.914</b>
	MAE $\downarrow$	0.019	0.022	0.023	<b>0.018</b>
ViSal	maxF $\uparrow$	0.949	0.947	0.933	<b>0.950</b>
	S $\uparrow$	0.948	0.947	0.938	<b>0.949</b>
	MAE $\downarrow$	0.014	0.016	0.017	<b>0.013</b>
VOS	maxF $\uparrow$	0.794	0.780	0.793	<b>0.801</b>
	S $\uparrow$	0.855	0.843	0.852	<b>0.855</b>
	MAE $\downarrow$	0.062	0.061	0.060	<b>0.060</b>

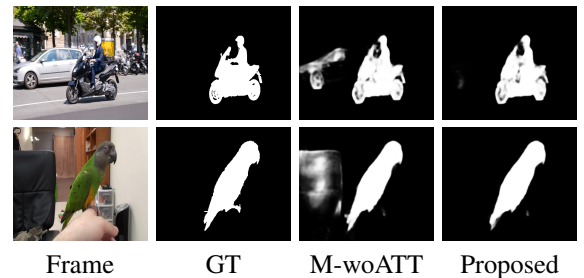


Fig. 9. Visual comparison of M-woATT and the proposed method.

denoted as CAA-BU which adopts a bottom-up fusion strategy, i.e., the spatial and temporal features at the same scale are fused and progressively fed into coarser scale. The results of these three variants and the proposed model are shown in Table V. The proposed module shows significant performance gain on three datasets by average performance promotion of 0.63%, 1.53%, 1.91% in maxF and 0.22%, 0.88%, 1.10% in S-measure compared with CAA-woS, CAA-woN and CAA-BU respectively. Moreover, we can also find that the nonlinear operation plays a more important role for SOD task compared with softmax operation. We ascribe it to the ability of getting rid of noisy features. And the top-down fusion strategy also brings large performance gain compared with the bottom-up fusion strategy.

3) Coarse Saliency Map based Operations: Note that the coarse saliency maps play a significant role in the proposed method. As analyzed in Section III-D, the multiple supervision and weighted aggregation of coarse saliency maps can further guide the network to generate more effective weights. The fused spatiotemporal feature can also be enhanced by spatial attention based on aggregated coarse saliency map. To evaluate the effectiveness of these operations based on coarse saliency map, we conducted a group of ablation experiments: M-SS represents the model trained in a single supervision manner; M-AGGS denotes a simplified coarse saliency aggregation method which aggregates the spatial and temporal coarse saliency maps by direct addition; M-woATT denotes the model without spatial attention. As shown in Table VI, the multiple supervised training process outperforms single supervision by

TABLE VI  
ABLATION STUDY OF THE COARSE SALIENCY BASED OPERATIONS.

		M-SS	M-AGGS	M-woATT	Proposed
DAVIS	maxF $\uparrow$	0.882	0.877	0.884	<b>0.891</b>
	S $\uparrow$	0.910	0.905	0.911	<b>0.914</b>
	MAE $\downarrow$	0.022	0.021	0.019	<b>0.018</b>
ViSal	maxF $\uparrow$	0.950	0.946	0.943	<b>0.950</b>
	S $\uparrow$	0.949	0.942	0.945	<b>0.949</b>
	MAE $\downarrow$	0.014	0.016	0.014	<b>0.013</b>
VOS	maxF $\uparrow$	0.794	0.789	0.795	<b>0.801</b>
	S $\uparrow$	0.854	0.851	0.854	<b>0.855</b>
	MAE $\downarrow$	<b>0.056</b>	0.063	0.061	0.060

1.02% in maxF and 0.44% in S-measure on DAVIS dataset. The weighted aggregation of coarse saliency maps brings an average increment of 1.18% in maxF and 0.74% in S-measure, validating its effectiveness. As for the spatial attention, it brings an average performance improvement by 0.76% in maxF and 0.29% in S-measure on three datasets. The final saliency map of the proposed DS-Net and M-woATT is shown in Fig. 9. The proposed saliency maps contain less background noise and enjoy higher accuracy, which also demonstrate the effectiveness of the proposed spatial attention.

## V. CONCLUSION

Noticing the high variation on the reliability of static and motive saliency cues for video salient object detection, in this paper, we propose a dynamic spatiotemporal network (DS-Net) to complementarily aggregate spatial and temporal information. Unlike existing methods that treat saliency cues in an indiscriminate way, the proposed algorithm is able to automatically learn the relative reliability of spatial and temporal information and then carry out dynamic fusion of features as well as coarse saliency maps. Specifically, a dynamic weight generator and a top-down cross attentive aggregation approach are designed to obtain dynamic weights and facilitate complementary aggregation. Extensive experimental results on five benchmark datasets show that our DS-Net achieves superior performance than state-of-the-art video salient object detection algorithms.

## REFERENCES

- [1] R. Zhao, W. Ouyang, and X. Wang, "Unsupervised salience learning for person re-identification," in IEEE CVPR, 2013, pp. 3586–3593.
- [2] H. Lee and D. Kim, "Salient region-based online object tracking," in 2018 IEEE Winter Conference on Applications of Computer Vision (WACV), 2018, pp. 1170–1177.
- [3] L. Itti, "Automatic foveation for video compression using a neurobiological model of visual attention," IEEE Transactions on Image Processing, vol. 13, no. 10, pp. 1304–1318, 2004.
- [4] H. Song, W. Wang, S. Zhao, J. Shen, and K.-M. Lam, "Pyramid dilated deeper convlstm for video salient object detection," in ECCV, 09 2018, pp. 744–760.
- [5] G. Li, Y. Xie, T. Wei, K. Wang, and L. Lin, "Flow guided recurrent neural encoder for video salient object detection," in IEEE CVPR, 2018, pp. 3243–3252.
- [6] D. Fan, W. Wang, M. Cheng, and J. Shen, "Shifting more attention to video salient object detection," in IEEE CVPR, 2019, pp. 8546–8556.
- [7] W. Wang, J. Shen, and L. Shao, "Video salient object detection via fully convolutional networks," IEEE Transactions on Image Processing, vol. 27, no. 1, pp. 38–49, 2018.
- [8] L. Itti, C. Koch, and E. Niebur, "A model of saliency-based visual attention for rapid scene analysis," IEEE Transactions on Pattern Analysis and Machine Intelligence, vol. 20, no. 11, pp. 1254–1259, 1998.
- [9] H. Li, G. Chen, G. Li, and Y. Yu, "Motion guided attention for video salient object detection," in IEEE ICCV, 2019, pp. 7273–7282.
- [10] J. Zhao, J. Liu, D. Fan, Y. Cao, J. Yang, and M. Cheng, "Egnet: Edge guidance network for salient object detection," in IEEE ICCV, 2019, pp. 8778–8787.
- [11] C. Deng, X. Yang, F. Nie, and D. Tao, "Saliency detection via a multiple self-weighted graph-based manifold ranking," IEEE Transactions on Multimedia, vol. 22, no. 4, pp. 885–896, 2020.
- [12] G. Ma, C. Chen, S. Li, C. Peng, A. Hao, and H. Qin, "Salient object detection via multiple instance joint re-learning," IEEE Transactions on Multimedia, vol. 22, no. 2, pp. 324–336, 2020.
- [13] C. Chen, S. Li, H. Qin, Z. Pan, and G. Yang, "Bilevel feature learning for video saliency detection," IEEE Transactions on Multimedia, vol. 20, no. 12, pp. 3324–3336, 2018.
- [14] M. Xu, B. Liu, P. Fu, J. Li, and Y. H. Hu, "Video saliency detection via graph clustering with motion energy and spatiotemporal objectness," IEEE Transactions on Multimedia, vol. 21, no. 11, pp. 2790–2805, 2019.
- [15] Y. Li, S. Li, C. Chen, A. Hao, and H. Qin, "Accurate and robust video saliency detection via self-paced diffusion," IEEE Transactions on Multimedia, vol. 22, no. 5, pp. 1153–1167, 2020.
- [16] Y. Gu, L. Wang, Z. Wang, Y. Liu, M. Cheng, and S. Lu, "Pyramid constrained self-attention network for fast video salient object detection," in The Thirty-Fourth AAAI Conference on Artificial Intelligence, 2020, pp. 10 869–10 876.
- [17] Y. Xue, X. Guo, and X. Cao, "Motion saliency detection using low-rank and sparse decomposition," in 2012 IEEE International Conference on Acoustics, Speech and Signal Processing (ICASSP), 2012, pp. 1485–1488.
- [18] W. Wang, J. Shen, and L. Shao, "Consistent video saliency using local gradient flow optimization and global refinement," IEEE Transactions on Image Processing, vol. 24, no. 11, pp. 4185–4196, 2015.
- [19] F. Guo, W. Wang, J. Shen, L. Shao, J. Yang, D. Tao, and Y. Y. Tang, "Video saliency detection using object proposals," IEEE Transactions on Cybernetics, vol. 48, no. 11, pp. 3159–3170, 2018.
- [20] Y. Wei, X. Liang, Y. Chen, X. Shen, M. Cheng, J. Feng, Y. Zhao, and S. Yan, "Stc: A simple to complex framework for weakly-supervised semantic segmentation," IEEE Transactions on Pattern Analysis and Machine Intelligence, vol. 39, no. 11, pp. 2314–2320, 2017.
- [21] L. Jiang, M. Xu, T. Liu, M. Qiao, and Z. Wang, "Deepvps: A deep learning based video saliency prediction approach," in ECCV, 2018, pp. 625–642.
- [22] P. Yan, G. Li, Y. Xie, Z. Li, C. Wang, T. Chen, and L. Lin, "Semi-supervised video salient object detection using pseudo-labels," in IEEE ICCV, 2019, pp. 7283–7292.
- [23] L. Chen, G. Papandreou, F. Schroff, and H. Adam, "Rethinking atrous convolution for semantic image segmentation," CoRR, vol. abs/1706.05587, 2017.
- [24] K. He, X. Zhang, S. Ren, and J. Sun, "Deep residual learning for image recognition," in IEEE CVPR, jun 2016, pp. 770–778.
- [25] G. Li, Y. Xie, L. Lin, and Y. Yu, "Instance-level salient object segmentation," in IEEE CVPR, 2017, pp. 247–256.
- [26] E. Ilg, N. Mayer, T. Saikia, M. Keuper, A. Dosovitskiy, and T. Brox, "FlowNet 2.0: Evolution of optical flow estimation with deep networks," in IEEE CVPR, 2017, pp. 1647–1655.
- [27] Q. Hou, M. Cheng, X. Hu, A. Borji, Z. Tu, and P. H. S. Torr, "Deeply supervised salient object detection with short connections," IEEE Transactions on Pattern Analysis and Machine Intelligence, vol. 41, no. 4, pp. 815–828, 2019.
- [28] P. Zhang, D. Wang, H. Lu, H. Wang, and X. Ruan, "Amulet: Aggregating multi-level convolutional features for salient object detection," in IEEE ICCV, 2017, pp. 202–211.
- [29] X. Wei, T. Zhang, Y. Li, Y. Zhang, and F. Wu, "Multi-modality cross attention network for image and sentence matching," in IEEE CVPR, 2020, pp. 10 938–10 947.
- [30] L. Ye, M. Rochan, Z. Liu, and Y. Wang, "Cross-modal self-attention network for referring image segmentation," in IEEE CVPR, 2019, pp. 10 494–10 503.
- [31] O. Russakovsky, J. Deng, H. Su, J. Krause, S. Satheesh, S. Ma, Z. Huang, A. Karpathy, A. Khosla, M. S. Bernstein, A. C. Berg, and F. Li, "Imagenet large scale visual recognition challenge," International Journal of Computer Vision, vol. 115, no. 3, pp. 211–252, 2015.

- [32] L. Wang, H. Lu, Y. Wang, M. Feng, D. Wang, B. Yin, and X. Ruan, "Learning to detect salient objects with image-level supervision," in *IEEE CVPR*, 2017, pp. 3796–3805.
- [33] F. Perazzi, J. Pont-Tuset, B. McWilliams, L. Van Gool, M. Gross, and A. Sorkine-Hornung, "A benchmark dataset and evaluation methodology for video object segmentation," in *IEEE CVPR*, 2016, pp. 724–732.
- [34] T. Brox and J. Malik, "Object segmentation by long term analysis of point trajectories," in *ECCV*, 2010, pp. 282–295.
- [35] P. Chockalingam, N. Pradeep, and S. Birchfield, "Adaptive fragments-based tracking of non-rigid objects using level sets," in *IEEE ICCV*, 2009, pp. 1530–1537.
- [36] D. P. Kingma and J. Ba, "Adam: A method for stochastic optimization," in *ICLR*, 2015.
- [37] F. Li, T. Kim, A. Humayun, D. Tsai, and J. M. Rehg, "Video segmentation by tracking many figure-ground segments," in *IEEE ICCV*, 2013, pp. 2192–2199.
- [38] D. Fan, M. Cheng, Y. Liu, T. Li, and A. Borji, "Structure-measure: A new way to evaluate foreground maps," in *IEEE ICCV*, 2017, pp. 4558–4567.
- [39] R. Achanta, S. Hemami, F. Estrada, and S. Susstrunk, "Frequency-tuned salient region detection," in *IEEE CVPR*, 2009, pp. 1597–1604.
- [40] J. Zhang, S. Sclaroff, Z. Lin, X. Shen, B. Price, and R. Mech, "Minimum barrier salient object detection at 80 fps," in *IEEE ICCV*, 2015, pp. 1404–1412.
- [41] W. Tu, S. He, Q. Yang, and S. Chien, "Real-time salient object detection with a minimum spanning tree," in *IEEE CVPR*, 2016, pp. 2334–2342.
- [42] T. Xi, W. Zhao, H. Wang, and W. Lin, "Salient object detection with spatiotemporal background priors for video," *IEEE Transactions on Image Processing*, vol. 26, no. 7, pp. 3425–3436, 2017.
- [43] Y. Chen, W. Zou, Y. Tang, X. Li, C. Xu, and N. Komodakis, "Scom: Spatiotemporal constrained optimization for salient object detection," *IEEE Transactions on Image Processing*, vol. 27, no. 7, pp. 3345–3357, 2018.
- [44] Y. Tang, W. Zou, Z. Jin, Y. Chen, Y. Hua, and X. Li, "Weakly supervised salient object detection with spatiotemporal cascade neural networks," *IEEE Transactions on Circuits and Systems for Video Technology*, vol. 29, no. 7, pp. 1973–1984, 2019.